# Ionic distribution around simple *B*-DNA models II. Deviations from cylindrical symmetry

Juan Carlos Gil Montoro and José L. F. Abascal
*Departamento de Química-Física, Facultad de Ciencias Químicas, Universidad Complutense de Madrid, E-28040 Madrid, Spain*

(Received 22 July 1997; accepted 16 June 1998)

The structure of the ions around two *B*-DNA models with added monovalent salt at the continuum solvent level is investigated by computer simulation. The salt concentrations cover a wide range, from 0.05 to 4.5 M. The simplicity of the so-called grooved primitive model (unit electron charges at the phosphate positions of canonical DNA and the grooves shape approximated by means of simple geometric elements) enables a detailed study of the counterion and coion distributions with a very small statistical noise. The inhomogeneity of the ionic distributions is noticeable along the axial direction up to distances of about 20 Å from the DNA axis. The counterions deeply penetrate into the DNA grooves even at very low added salt concentrations. In the minor groove, the counterions are preferentially located in its center whereas they lie at the sides of the major groove, close to the phosphate positions. The coions also enter within the major groove, especially in the systems at high added salt concentrations for which regions of absolute negative charge can be found within the groove. This can be explained in terms of an arrangement of ions with alternating charges. The grooved primitive model has also been solved in the context of the finite difference Poisson–Boltzmann theory. The theory accurately describes the ionic structure around DNA at low salt concentrations but the results deteriorate with increasing salt missing important qualitative features at or above molar concentrations. The other model investigated differs from the more detailed one in that the shape of DNA is not taken into account; a soft cylinder is used instead. The counterions accumulate in this model in front of the phosphates and the axial inhomogeneity of the distribution quickly vanishes. These results together with those of previous investigations lead to the conclusion that the *coupling* of the discrete description of the DNA charge with the steric effects due to the presence of the grooves is the primary determinant of the final ionic distribution, especially at high salt concentrations. This effect may play a decisive role in those DNA properties which are strongly dependent on the salt concentration, like the *B*- to *Z*-DNA conformational transition.  [S0021-9606(98)50336-4]

## I. INTRODUCTION

The physico-chemical properties and biological function of DNA in solution are dictated by its polyelectrolyte nature, and thus, they are strongly influenced by salt conditions. The binding interactions of proteins and other ligands to DNA often show a dramatic salt dependence.[1,2] The DNA melting temperature depends on salt concentration too.[3] In fact, ionic effects play a central role at all levels of DNA structural organization.[4] In particular, the reversible transition between the *B* and *Z* forms of DNA,[5–9] which may have a significant biological role,[10–12] can be induced by adding salt to the solution. Some of these properties, such as osmotic pressure, activity coefficients or Donnan equilibria,[13] depend essentially on the mean electrostatic field far from the polyion which is in turn dependent on *how many* ions (counterions mainly) are close to the DNA molecule. These bulk or ''macroscopic'' properties have been successfully explained in terms of very crude DNA models like the line of charge of the counterion condensation theory of Manning,[14–17] or the Poisson–Boltzmann theory applied to a homogeneously charged cylinder.[18–20] The latter model has been thoroughly investigated by Monte Carlo computer simulation.[20–24] Nevertheless, there is another class of properties which depend not only on how many ions are in the DNA proximity but also on *where* are those ions placed relative to the DNA structure, i.e., whether the ions penetrate into the grooves or not, whether they remain tightly bound to certain DNA sites or are able to diffuse, and whether they lose their coordination solvent sphere. The above mentioned salt-induced transition between the *B* and *Z* forms of DNA, the release of metal cations in the binding of ligands and proteins to DNA[25] or the diffusion and conductivity properties of DNA/salt systems are only a few examples. It is for these properties that knowledge of the detailed distribution of ions near DNA is of crucial importance, and one is forced to go beyond homogeneously charged models to others in which the DNA inhomogeneity is taken into account.

Unfortunately, the experimental determination of ion distributions around DNA seems very difficult. Although the global counterion decay in salt-free DNA systems has been recently determined by small-angle neutron scattering,[26,27] the situation near DNA and/or with added salt is more complex. The region close to the polyelectrolyte can be probed by the quenching effect of counterions over fluorescent

 

polyelectrolytes[28] or by the enhancement by the polyelectrolyte of energy transfer between counterions.[29] Nevertheless, these techniques are unable to resolve the anisotropy of the ionic distribution because they give only a cylindrically averaged information. Crystal x-ray studies may serve as a guide, but one has to be cautious as the structure in solution—the relevant state to DNA/salt systems—may be quite different from that of the crystal where the high DNA concentration induces cooperative effects (packing, electrostatic) among several molecules. Besides, the location of counterions in x-ray assignments tends to be uncertain. The most promising technique is $^{23}Na^{+}$ nuclear magnetic resonance (NMR) spectroscopy. The sodium nucleus relaxes its quadrupole moment via a coupling with electric field gradients in its vicinity, and thus may serve for the determination of sodium population close to DNA.[30] Unfortunately, NMR data is difficult to interpret unequivocally in terms of structure. Often, the analysis makes use of theoretical limiting results, such as those from the counterion condensation theory of Manning, or requires the aid of a molecular mechanics package.[31]

An alternative to direct experiments are simulation techniques. In principle, it is possible to simulate a system consisting of a long DNA molecule, its corresponding counterions, added salt, and solvent particles. In practice, this task is at present exceedingly difficult, especially if series of simulations are required to assess the trends. Forester and McDonald[32] simulated an all-atom rigid DNA with water, counterions and five chloride coions, resulting in about 0.1 M added-salt concentration. Sometimes a single dimethylphosphate unit has been used[33] but important cooperative effects are not considered in that case. Additionally, several salt-free (no added salt) simulations of DNA oligomers at the atomic level have been carried out (for a review on all-atom DNA molecular-dynamics simulations see Ref. 34). Explicit inclusion of counterions produces convergence problems[35] which may be enhanced with the addition of salt. Other handicaps of all-atom DNA simulations are the strong dependence of the results on the initial conditions[32,35] as a result of the high particle density in combination with the system inhomogeneity. The impossibility of including a consistent axial mean-field long-range potential in systems with explicit water has also been pointed out.[36] For these reasons, in the context of biophysical studies like drug-DNA or protein-DNA binding, few simulation studies have been conducted at the explicit water level of detail.[37] In essence, the above difficulties arise from the insufficiency of the actual computational power and may be in course of solution in the future. From our point of view, there is a deeper shortcoming in using such detailed models. The interplay between the different forces acting on each particle makes very difficult the assessment of the importance of each interaction. It is then very hard to ascribe a given effect to a particular interaction. Moreover, the subtle competition between them makes it possible that similar simulation studies lead to contradictory results.[38] We have, therefore, turned our attention back to simple models since they allow us to learn the physics that a given refinement adds with respect to a previous level, and thus to unambiguously assign each effect to its cause.

At the McMillan–Mayer level, the effect of water is introduced as a modification of the electrostatic interaction between charges by means of a dielectric function. These so-called continuum models offer a viable alternative both for the understanding of the ionic atmosphere around DNA[39] and for molecule–DNA interactions.[35] The advantages are a drastic diminution in the number of particles, which enables the extension of the range of applicability of the simulations, going beyond the salt-free case and allowing larger runs. Additionally, grand canonical ensemble simulations become feasible. The penalty is that effects due to the microscopic heterogeneity of water such as hydration, solvation, and hydrogen bonding are missing, although some of them may be partially accommodated by the model. For example, the hydration sphere is usually accounted for through an increase in the ionic effective radius. In a previous paper[40] (hereafter referred to as paper I) we have explored cylindrically averaged properties for several simple *B*-DNA models. We dealt both with homogeneously and discretely charged polyelectrolytes. An important result of paper I was that the effect of the DNA charge discretization may be important when coupled to the steric hindrance due to the polyion grooved shape. In fact, for a quite simple grooved model, the results were compatible with a number of DNA properties, such as excluded volume and concentration profiles. More importantly, ionic distributions compared favorably with those from all-atom DNA simulations and exhibited typical features of such complex models. The cylindrically averaged properties previously investigated have not the natural symmetry of the (helical) DNA charge distribution. It seems then interesting to study the deviations from the cylindrical symmetry. Apart from the intrinsic interest of such study, an additional motivation is that we expect to obtain some insights for a better understanding of the DNA conformational transitions.

An alternative route for solving this sort of systems is the Poisson–Boltzmann (PB) approximation.[41,42] Being orders of magnitude cheaper in terms of computer time than the direct simulation, the PB theory has become very popular in recent years, particularly in the context of all-atom DNA models.[43–45] This theory predicts counterion profiles close to the macromolecule that are around a 10%–15% lower than the simulation results for cylindrical homogeneously charged DNA models and salt-free conditions or at low monovalent salt concentration.[20,21] Nevertheless the accuracy of the PB calculations for more refined DNA models and/or at high salt has not been clearly assessed.

In this work we analyze the distribution of ions around two discretely charged models of *B*-DNA over a wide range of monovalent salt concentration via computer simulation. Our object is to address the specific ionic organization in the vicinity of DNA which is likely to be produced by the discrete nature of the charge as opposed to the radially symmetric profiles given by homogeneously charged models. We focus our interest on the simple grooved model described below and pay special attention to the high salt regime. Besides, we want to know whether an even more simple DNA

model (a repulsive cylinder with discrete charges) is able to reproduce the main predicted features of the ionic structure close to DNA. The motivation for this is to assess the suggestion that the discretization of the charges is not sufficient to explain the DNA behavior because the polyelectrolyte shape plays an important structural role. Additionally, the grooved model has been solved using the PB approach at different salt concentrations in order to check its predictions against the simulation results. In Sec. II we describe the DNA models used in this work and address methodological details of the simulations and the Poisson–Boltzmann calculations. The results are presented in Sec. III, and the conclusions are summarized at the end of the paper.

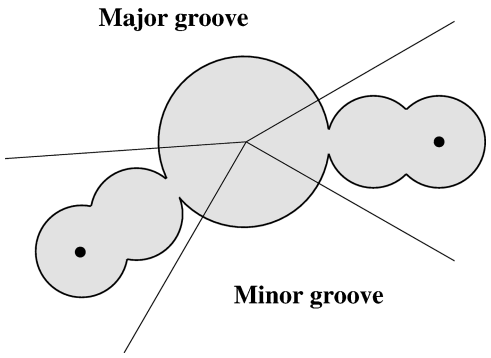


FIG. 1. Cross section of the grooved primitive model of DNA. Both pairs of spheres are drawn at the same height, although in the model they are 0.78 Å apart.

## II. DNA MODELS AND METHODOLOGICAL DETAILS

Only discretely charged DNA models are considered in this work. As most of the DNA charge lies at the phosphate groups,[46] unit negative charges are placed in both models at the phosphorus positions. For canonical *B*-DNA, these can be written in a compact form in cylindrical coordinates as[47]

$$\begin{aligned} \rho_i^s &= 8.91, \\ \phi_i^s &= \phi_0^s + 36 \cdot i, \\ z_i^s &= z_0^s + 3.38 \cdot i, \end{aligned} \tag{2.1}$$

where $s=1,2$ specifies the nucleic acid strand, and thus, $i=0,\ldots,9$ describes a complete DNA helix turn. The radial and axial distances to the helix center, $\rho$ and $z$, are given in angstroms and the angular coordinate, $\phi$, in degrees. Besides, $\phi_0^s$ and $z_0^s$ are both zero for the phosphates in the first strand, and 154.4° and 0.78 Å, respectively, for those in the second one.

Two DNA models are considered, both previously addressed in paper I, the grooved primitive model (GP model), and a discretely charged soft cylinder (DS model). In the latter, the charges are embedded within the DNA core whose surface appears smooth and continuous to the solution (mobile) ions. The GP model, on the other hand, incorporates the accessibility of the DNA grooves to the mobile ions in a computationally tractable way.[40] This model was obtained by fitting a set of geometrically simple objects to the shape of a DNA molecule with a couple of restrictions. The procedure is amply discussed in paper I. A section of the resulting model is depicted in Fig. 1. A cylinder mimics the central core of DNA, totally inaccessible to the mobile ions, while each nucleotide is completed by two identical spheres, one of them—the phosphate sphere—centered at the charge positions, Eq. (2.1), and the other—the intermediate sphere—lying between the phosphate and the cylinder at $\rho=5.90$ Å.

Irrespective of whether the ions are fixed (the polyelectrolyte charged sites) or mobile (the solution particles), the repulsive interaction between ions is a soft potential of the form

$$U_{ij}^{\mathrm{rep}}(r_{ij}) = K_{ij}\frac{1}{r_{ij}^n}, \tag{2.2a}$$

$$K_{ij} = \frac{A_M |z_i z_j| e^2}{N_c n}(r_i + r_j)^{(n-1)}, \tag{2.2b}$$

$r_{ij}$ being the distance between ions $i$ and $j$. The choice of $A_M=1.7476$ (the Madelung's constant of the NaCl solid structure), and $N_c=6$ (the coordination number of the same structure) together with the value $r_i=1.4214$ Å (the nominal radius of ion $i$) taken for both anions and cations, gives bulk electrolyte properties approximately corresponding to a restricted primitive model with hard-sphere diameters of 4.2 Å.[48] This size has been used in other recent electrolyte solution studies[23,49–52] and roughly corresponds to a sodium ion with the account of its hydration shell.[49,53] There is large evidence that sodium ions do not lose their hydration spheres in their association with DNA.[32,54] Additionally, the intermediate spheres of the GP model interact with the mobile ions through the same repulsive potential that acts on them, i.e., Eq. (2.2).

The repulsive potential for the central cylinder of the GP model is of the form

$$U_{ip}^{\mathrm{rep,displaced}}(\rho_{ip}) = K'_{ip}\frac{1}{(\rho_{ip}-\rho_0)^n}, \tag{2.3}$$

where $n=9$, $K'_{ip}=2.7291\cdot 10^{-17}$ J·Å,[9] and $\rho_0=2.91$ Å corresponding to a grooves depth of about 3.9 Å, consistent with previous estimates (between 3.5 and 4 Å[55]). The repulsive potential for the DS model is merely a cylindrical soft potential of the same form but the origin of the repulsion coincides now with the radial position of the charges, $\rho_0=8.91$ Å. This results in the maximum of the radial distribution of counterions appearing at about 12 Å, the usual closest approach distance in hard rod DNA simulations.

Although dielectric effects induced by the polyelectrolyte may be rather complex in its vicinity,[56] we use the Coulombic potential—without further modification beyond the mere consideration of the dielectric constant of water—for the interactions between mobile ions. The justification for this approximation is given in paper I. The electrostatic potential is just

$$U_{ij}^{\mathrm{cou}} = \frac{z_i z_j}{4\pi\epsilon_0\epsilon}\frac{e^2}{r_{ij}}, \tag{2.4}$$

where $e$ is the magnitude of the electronic charge, $\epsilon_0$ the vacuum permittivity, $\epsilon = 78.358$ the (relative) dielectric constant of the solvent (water at 25 °C), and $z_i$ and $z_j$ the ionic electrovalences of the interacting ions. Only monovalent ions are considered in this work.

As for the DNA–ion interaction, it is well established in computer simulations of charged inhomogeneous systems that the interactions of each particle with the part of the system along the directions in which periodic boundary conditions are used must be included. This is due to the fact that the anisotropic charge distribution is repeated *ad infinitum* in those directions. The most used and successful method for including this long-range axial interaction for polyelectrolyte models in which the charge is homogeneously distributed was pioneered by Torrie and Valleau for the case of the planar electrical double layer.[57] There, the effect of the charge distribution outside the simulation cell is included as a mean-field term computed self-consistently from the average charge distribution within the cell. The appropriate formulas are given, for example, in Ref. 58. The equivalence of the results obtained with this procedure and those using the Ewald summation method, traditionally used in the simulations of homogeneous Coulombic systems, was shown in Ref. 58.

Nevertheless, when the polyelectrolyte is made up of discrete charges, the long-range correction formulas used for the homogeneous charge are no longer valid, and an alternative procedure must be used.[59] In this case, the electrostatic field can be obtained as that of a sum of arrays of discrete charges placed along lines parallel to the DNA axis. The potential between an ion $i$ and an infinitely long array of discrete charges is[59]

$$U_{i\nu}^{\text{array,inf}}(\rho_{i\nu},\Delta z_{i\nu}) = 2z_i\xi_\nu\beta^{-1}\left[\log(\rho_{i\nu}) - 2\sum_{j=1}^{\infty} K_o(\kappa_j\rho_{i\nu})\cos(\kappa_j\Delta z_{i\nu})\right], \tag{2.5}$$

where $\rho_{i\nu}$ is the distance from the ion to the array $\nu$, $\xi_\nu$ the reduced axial charge density of the line, $\kappa_j = 2\pi j/b_\nu$ ($b_\nu$ being the distance between the consecutive charges in the array), $\Delta z_{i,\nu}$ the axial coordinate of the ion with respect to the closest charged site of the array, and $K_o$ is the modified Bessel function of order zero and second kind. Equation (2.5) is obtained by expanding the point-charge potentials in cylindrical coordinates.[60] The first term is the potential of an infinite homogeneous line of charge and the second is the charge discreteness contribution. The summation in the right hand side is quickly convergent, so few terms are needed provided that $\rho_{i\nu}$ is not too close to zero. In the limit $\rho_{i\nu} \to 0$, Eq. (2.5) transforms into a more convenient relation (see Ref. 59 for details).

The total potential between the charges in an infinite DNA helix and a mobile ion is then

$$U_{ip}^{\text{sites},\infty} = \sum_\nu U_{i\nu}, \tag{2.6}$$

where the sum extends over the 20 arrays of charge (in the case of our $B$-DNA models, there are twenty charged sites—10 phosphorus atoms in each of the strands—and thus $\xi_\nu = \xi/20$). In this way, the above equation can be more efficient than the explicit sum over each of the polyelectrolyte charged sites for simulation cells made of three or more turns along the axial direction. More importantly, this procedure treats in a consistent manner the long-range axial potential as it includes the interactions with all the polyion charges. In this regard, it is important to notice that the usual method of summing explicitly the coulombic interactions within the simulation cell and adding a long-range correction assuming a homogeneous charge distribution outside the cell is inconsistent and leads to erroneous results.[59]

As to the periodic boundary conditions for the radial direction, two different methods have been employed. In the diluted cases at 0.05 M, the traditional cell model[61]—consisting in a (hard) cylindrical boundary limiting the space available to the ions—is a satisfactory option. More concentrated salt solutions are, on the other hand, significantly affected by the presence of the hard boundary,[40,58] which results in a spurious attractive potential.[62] For these systems, the modulated bulk as fuzzy boundary method[58] (MBFB), which has proved its usefulness in the simulation of long-ranged inhomogeneous systems, has been used instead. In this method, the cylinder corresponding to the cell model (the inhomogeneous region) is immersed in a periodic box (an hexagonal prism in our case) filled with bulk solution and the hard wall removed, so that mobile ions are able to cross the boundary. The ions interact with the surrounding bulk through a discrete particle–particle modulated (short-ranged) Coulomb potential[63] while the missing tail is recovered as a mean-field contribution computed in a self-consistent way.

The Monte Carlo simulations cover a broad range of bulk concentrations, from 0.05 to 4.5 M. The simulated states are given in Table I. We will refer to each simulation by its nominal concentration, keeping in mind that the actual bulk salt concentration is that observed in the simulation far away from the polyelectrolyte. The bulk concentrations are also shown in Table I. In the concentrated systems (1–4.5 M), classical Metropolis sampling has been used. In diluted polyelectrolyte systems convergence problems of the Markov chain can occur.[64] This is due to the strong inhomogeneity of the counterion distribution, which changes from about one molar concentration near DNA to the corresponding bulk value which is several orders of magnitude smaller at low added-salt concentrations. To solve this problem, a density scaled sampling scheme was proposed by Gordon and Goldman.[64] In this method, the ion trial displacement parameter varies with the distance to the polyelectrolyte; it is small near it and large far away. The method is able to furnish reasonable acceptance rates (in the range 0.3–0.6) at any separation from the polyelectrolyte axis. Of course, the acceptance algorithm must be modified accordingly.[64] We have employed the density scaled sampling in the simulations at 0.05 M. Additional simulation details can be found in paper I.

The finite difference Poisson–Boltzmann (FDPB)[41,65]

TABLE I. The simulations.

| DNA model | Nominal concentration (M) | Radial boundary | Number of ions[a] | Radial dimension (Å)[b] | Bulk concentration (M)[c] |
|---|---|---|---|---|---|
| Discretely charged soft cylinder (DS) | 1 | MBFB | 40+310 | 36.0 | 0.949 |
| Grooved primitive model (GP) | 0.05 | Cell | 60+120 | 118.3 | 0.0486 |
| | 1 | MBFB | 40+205 | 32.5 | 0.989 |
| | 2.5 | MBFB | 20+194 | 22.0 | 2.52 |
| | 4.5 | MBFB | 20+200 | 22.5 | 4.45 |

[a]DNA charge counteracting ions+added salt ion pairs.
[b]Cell radius in the cell model simulation and internal region radius in the MBFB simulations.
[c]Estimated uncertainties affect the last figure.

form of the PB equation has also been applied to the GP model of DNA. This approach requires the macromolecule to be modeled as a hard body impenetrable to the ions. Thus we need to establish an equivalence between the soft repulsions used in the simulations and the distances of minimum approach between the objects (cylinder and spheres) assumed by the GP model and the mobile ions. This has been done in paper I when a comparison between the excluded volume of atomic DNA and that of the GP model was reported. There, the hard ion diameter was regarded at first as equivalent to the distance at the potential minimum between unlike ions.[48] Nevertheless, this value was decreased by 0.5 Å to account for the increased ion condensation around DNA by virtue of the collective effect of its charges. The recipe has also been found suitable for the FDPB computations in order to ensure that the ion concentration profiles start at the same distance to the DNA axis as in the simulations. The dielectric constant of the polyelectrolyte is that of the solvent as in the simulations. The DELPHI program has been employed for the FDPB calculations.[65,66] We have used a cubic grid and a focusing technique starting with a grid extent of 101.4 Å corresponding to the height of three DNA helix turns. The potential values from this calculation are used as initial input to a second computation using a grid extent of one DNA turn, 33.8 Å. As a consequence of the high DNA charge, the potential changes abruptly in the vicinity of the polyion. A fine grid is required to avoid numerical errors in the solution of the PB equation which would lead to an incomplete neutralization of the DNA charge. We have used a cubic grid with 201 points per side giving a final resolution of 5.92 grid points per Å. In these conditions, the FDPB calculations require about the same computer time as the simulation runs.

## III. RESULTS

To present results for nonradially averaged ion distributions around DNA we may benefit from the helical arrangement of the phosphates. Previous all-atom studies have done so by projecting the concentration profiles onto the nearest base pair plane[39,67] in a spiral staircase manner. We propose to go further within a similar approach. If the charged sites form a continuous ridge, the concentration profiles would depend only on two coordinates. Every point could be projected onto the helical line defined by the ridge. A natural coordinate of the system is $\rho$. The other independent coordinate may be either the angle needed to reach the reference helix strand by moving on a constant $\rho$-$z$ circumference or the axial distance to the strand (see Fig. 2). Let us denote them $\delta\phi$ and $\delta z$, respectively. Notice that the points lying in the reference helix have their cylindrical coordinates related by $z=(L/360)\phi$, $L$ being the helix pitch ($L=33.8$ Å). An inspection of Fig. 2 enables us to write down the relationship between the cylindrical and the new helical coordinates

$$\delta\phi=\frac{360}{L}z-\phi \tag{3.1}$$

and

$$\delta z=\frac{L}{360}\phi-z. \tag{3.2}$$

The angular separation between the phosphates in both strands is then $\delta\phi=146.1°$ or, equivalently, $\delta z=13.7$ Å (depending on the choice of the strand origin the negative complementary values $\delta\phi=213.9°$, $\delta z=20.1$ Å may also be obtained).

Although the ridge is not continuous, the consecutive charged groups are so close that the effect of the discontinuity on the surrounding ion atmosphere is almost negligible (this ''helical projection'' is only marginally disrupted in the vicinity of the phosphates). Notice that when the ionic dis-

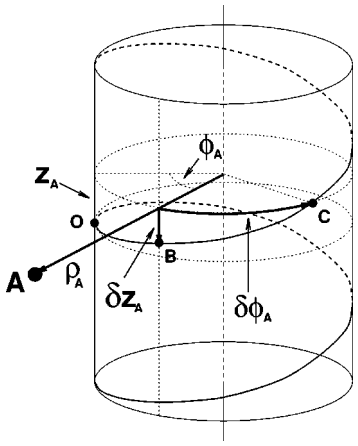


FIG. 2. Coordinates used in the helical projection. For a point A whose cylindrical coordinates are $\rho_A$, $\phi_A$, and $z_A$, only two coordinates are needed in the helical projection, $\rho_A$ and $\delta z_A$ (or, equivalently, $\delta\phi_A$). The new coordinate $\delta z_A$ (or $\delta\phi_A$) is obtained by moving along a constant $\rho$-$\phi_A$ line (or a constant $\rho$-$z_A$ circumference) in order to reach the reference helix strand at point B (or point C).

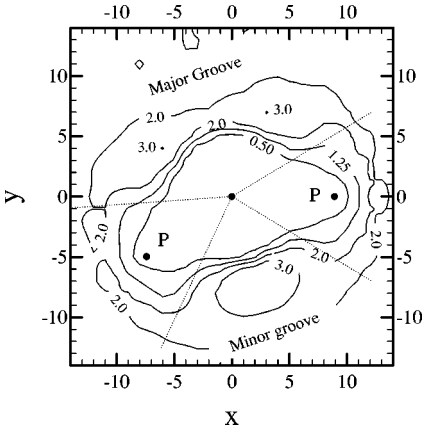


FIG. 3. Counterion distributions around the GP model at 1 M added salt concentration. The scale is molar units. The view corresponds to slabs perpendicular to the DNA axis with constant $\delta z$ [see Eq. (3.3) for $x$ and $y$ definitions]. The phosphates positions and the helix axis are marked by filled circles. The major and minor grooves are the regions in the top-left and bottom-right areas of the figure, respectively.

tribution is averaged in terms of the helical coordinates $\rho$ and $\delta\phi$, it is possible to express it in terms of Cartesian-type coordinates through the relations

$$x=\rho\ \cos(\delta\phi), \tag{3.3a}$$

$$y=\rho\ \sin(\delta\phi). \tag{3.3b}$$

Ion distributions were collected during the simulations, the helical projection was performed on the fly and accumulated in double entry $\rho$ and $\delta\phi$ histograms. One of these representations in the plane $(\delta x, \delta y)$ for counterions, GP model and at 1 M added salt is given in Fig. 3. The phosphate positions in both strands and the helix axis are marked by filled circles. The major and minor grooves are easily identified in the figure. The general shape of the curves is similar to that observed in Guldbrand *et al.* salt-free simulations with an all-atom DNA model.[39] The lack of radial symmetry is apparent from the representation. The highest counterion concentration is located in the minor groove. This effect seems to be a consequence of the very negative potential due to the proximity of both phosphates across the minor groove. This has also been observed in the salt-free simulations of Ref. 55 (where a DNA-shaped model was used[68]) and is predicted by both the SATK (solvent accessibility Tanford–Kirkwood)[69] and FDPB[41,70] treatments of DNA.

The same distribution but in the plane $(\rho, \delta z)$ is given in Fig. 4 where the radial coordinate refers to $\rho$ and the axial coordinate to $\delta z$. The satisfactory symmetry of the curves with respect to the middle of the grooves gives an idea of the small statistical errors involved in the simulations. Although this representation is perhaps less intuitive at a first glance, we prefer it as details appear more clearly than in the previous plot. There are three regions exhibiting local maxima in the counterion concentration. As commented above, the higher accumulation of counterions is located in the minor groove at a radial coordinate of about 7.5 Å. A second maximum in the counterion concentration appears in the major groove region. But contrarily to what happens in the minor one, the maximum is not located at the center of the groove

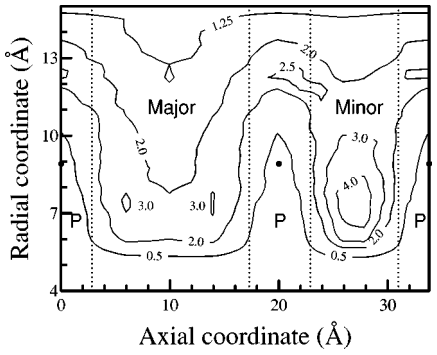


FIG. 4. The same distribution of Fig. 3 viewed in a cut through the DNA axis ($\delta\phi$ constant).

but it splits in two symmetrical maxima at the outer sides of the groove, close to the nearest phosphates. A third maximum is located in front of the phosphates at large radial coordinates. No counterions are found in the space between two adjacent phosphates along the ridge (in our representation, the projected coordinates of such locations are exactly coincident with those of the phosphates) which validates the assumption made to construct the helical projection in that the surrounding ion atmosphere is essentially the same as that of a continuous ridge. The shape of the 2.0 M contour plot is quite interesting. In the minor groove and the phosphates region, it deviates slightly from the cylindrical symmetry (i.e., it is almost flat) lying around 12 to 13 Å from the DNA axis, whereas the curve penetrates deeply into the major groove (as close as 8 Å from the DNA axis). The cylindrical symmetry of the counterion distribution is restored at a radial coordinate of about 20 Å (results not shown), as previously obtained in Poisson–Boltzmann studies.[42] Regarding the coion distribution (Fig. 5), the departures from the cylindrical symmetry are noticeable as they show some tendency to enter within the major groove. In the system at 1 M salt concentration, the 0.25 M coion contour plot approaches the DNA axis as close as 6 Å. Interestingly, the penetrability of the coions into the grooves is also significantly enhanced at high salt concentrations.

For brevity, and because of the reasons which will become more apparent later, we only sketch now the main features of the ionic atmosphere around DNA at salt concentrations as low as 0.05 M and as high as 4.5 M, because they

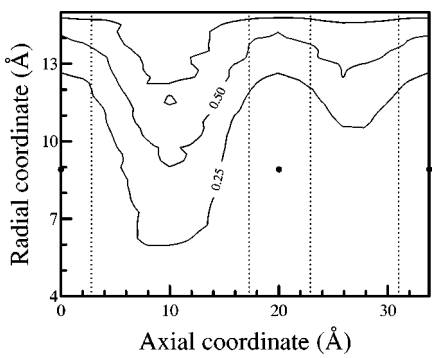


FIG. 5. Coion distributions around the GP model at 1 M added salt concentration.

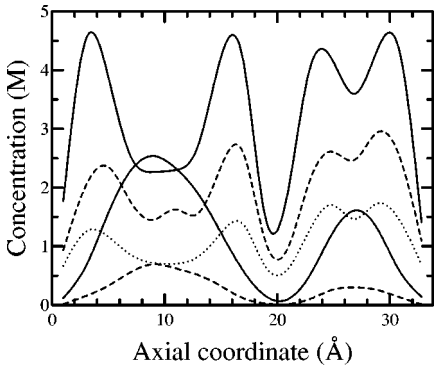


FIG. 6. Concentration profiles of coions and counterions for the GP model at a radial coordinate of 10.9 Å and different salt concentrations: 0.05 M (dotted line), 1 M (dashed lines), and 2.5 M (solid lines). The coion profile at 0.05 M is not visible on the scale of the figure.

exhibit similar trends to those of the previous figure despite the great differences in their bulk ionic strengths. Representative minor groove counterion concentrations are about 3 and 7.5 M, respectively, $\sim 3$ M over the bulk concentration, the same increment as in the 1 M salt concentration system where the minor groove concentration is 4 M. It is worth mentioning that the penetrability of the counterions into the major groove with respect to the minor is enhanced at higher ionic strengths. In fact, for the system at 4.5 M salt concentration, the peaks in the counterion concentration within both grooves are very similar.

From the comments in the preceding paragraph, it might be deduced that the counterion distribution is scarcely sensitive to the salt concentration beyond obvious changes in the number of condensed ions. This is not true though the variations are quite subtle. Figure 6 represents the variation with salt concentration of the counterion and coion profiles for the GP model at a radial coordinate of 10.9 Å, i.e., just in the shear surface of DNA.[71] The difference between the counterion concentrations at the edge and the center of the major groove increases with the addition of salt. The corresponding increase of the coion concentrations is more appreciable in the middle of the major groove. It is particularly strong from about 1 M salt concentration: When the added salt goes from 1 to 2.5 M

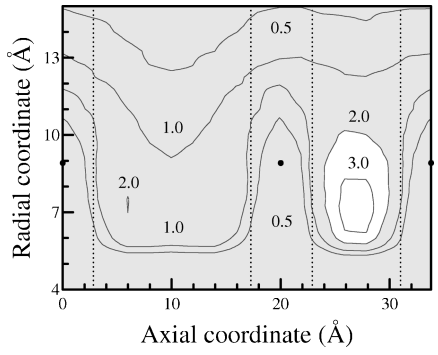


FIG. 7. Net charge profile (the difference between the counterion and the coion concentrations) for the system at 0.05 M salt concentration. The areas with net charge concentrations higher than 1 M are white and those between 0 and 1 M are grey shaded.

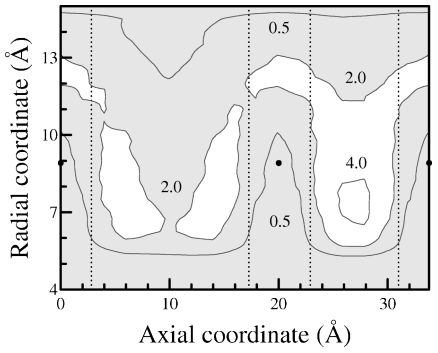


FIG. 8. Same as Fig. 7 but for the system at 1 M salt concentration.

and the number of coions within the groove (with $\rho < 11$ Å) per DNA base changes from 0.035 to 0.17. Since in this region the counterion concentration increases more slowly, we eventually arrive at the striking result that *coions outnumber counterions*. This is shown in Fig. 6 for the 2.5 M system at an axial coordinate of 9–11 Å. We will refer to this phenomenon as local charge inversion. A separate analysis of the counterion and coion profiles may then miss important structural trends.

A more representative idea of the ionic atmosphere around DNA is given by the net charge profile, which is simply the difference between the counterion and coion concentrations at any point because the solution cations and anions carry equal charges of opposite sign. Figures 7–10 display the net charge using the same representation as that of Figs. 4 and 5 for the counterion and the coion concentrations. The net charge function for the system at 0.05 M salt concentration (Fig. 7) is essentially coincident with the counterion concentration profile. The departures between the net charge and the counterion profile are noticeable only at very high added salt concentrations. This is clearly seen when one compares both results for the system at 1 M salt concentration (Figs. 8 and 4, respectively). Even at such high ionic strength, the differences are almost null in the minor groove region and not important in the major one. But at higher salt concentrations the situation changes dramatically. In the 2.5 M system (Fig. 9), the coion concentration in the outer region of the major groove exceeds that of the counterions, and, in the 4.5 M system, the region of negative charge deeply penetrates within the major groove (Fig. 10). At the

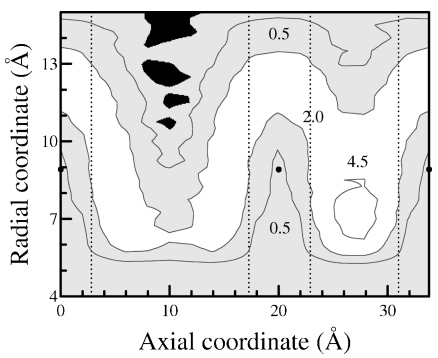


FIG. 9. Same as Fig. 7 but for the system at 2.5 M salt concentration. The areas with negative net charge concentrations are black.

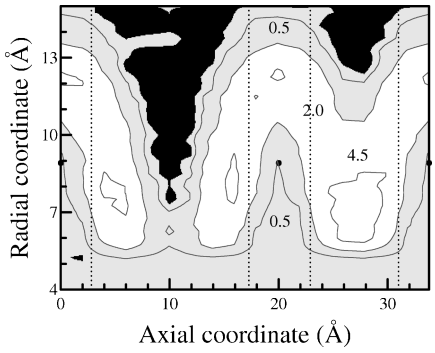


FIG. 10. Same as Fig. 7 but for the system at 4.5 M salt concentration.

latter salt concentration, the coions outnumber the counterions also in the vicinity of the minor groove. It is to be noticed that although the population of counterions within the minor groove exceeds that of the coions at any ionic strength, the concentration of the latter ions is far from negligible at high salt. There the coion concentration reaches values about 3 M in the system at 4.5 M bulk salt concentration. As the corresponding counterion concentration is close to 7.5 M, the net charge profile still shows an excess of positive charge within the minor groove.

Anions in the middle of the grooves of the GP model may be stabilized by the occurrence of alternating charge sign ion sequences of the type phosphate–counterion–coion–counterion–phosphate. A requirement for the formation of such an arrangement is that the groove should have enough room to accommodate three ions along the axial direction. The minor groove cannot accommodate three layers of ions, and it seems that the major groove also cannot hold them easily. Nevertheless, if the mobile anion is placed in the outer limit of the major groove, the steric conditions may be fulfilled. The alternating charge sequence also explains why the higher counterion concentration within the major groove is found at its sides.

The DS model gives an ionic distribution completely different from that obtained with the GP model. The counterion distributions for the system at 1 M salt concentration is presented in Fig. 11. The counterions cluster in front of the charged phosphates, almost in a site-bindinglike manner. This behavior has also been observed in the salt-free simulations of Ref. 55. The discrepancy between both models is more prominent if the number of counterions in different regions around DNA is considered. We assign an ion to the phosphates region if its angular separation from a phosphate (in the helical projection) is within $\pm 30$ degrees. With this definition three classes emerge, the phosphates region ($2 \times 60°$) and the major and minor groove regions (153.9° and 86.1°, respectively). The angular amplitude of the classes are in the relation 1.8:1.4:1 in the order major groove, phosphates and minor groove (the separation between classes is indicated by dotted lines in the preceding figures). In Fig. 12 we represent the number of counterions in each class for the GP and DS models at 0.05 M salt concentration as a function of the radial distance to the polyelectrolyte axis. The number of ions refer to a DNA base. In the DS model, the phosphates class contains more counterions than either of the grooves classes, while in the case of the GP model the opposite is true. The raise of the phosphates class curves in both models is so different that they cross at 13.9 Å. This behavior is remarkably salt-independent; at 1 M the cross point is at 13.3 Å (results not shown). As for the grooves counterion population, both models give qualitatively similar results. Only slightly more counterions are accommodated in the major groove class despite its much larger angular amplitude. This corresponds to the higher concentration found in the minor groove (as commented above), and is consistent with an x-ray crystallographic study by Bartenev *et al.*[72] on CsDNA, where an equal number of $Cs^+$ ions in both major and minor grooves was found. Of course, the actual number of ions in each class depend on the somewhat arbitrary angular amplitudes, though the chosen assignment seems coherent. The comments about the relative occupation of the classes by counterions for the 0.05 M system also apply to more concentrated solutions.

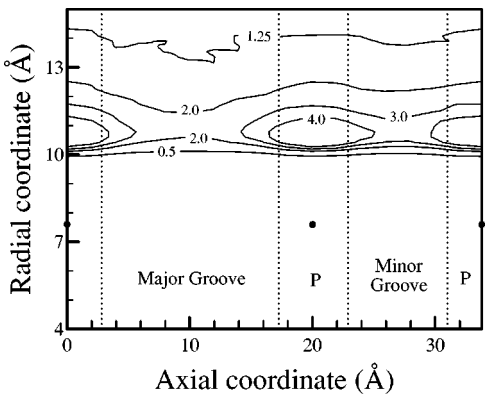


FIG. 11. Counterion distributions around the DS model at 1 M added salt concentration (to be compared with Fig. 4).

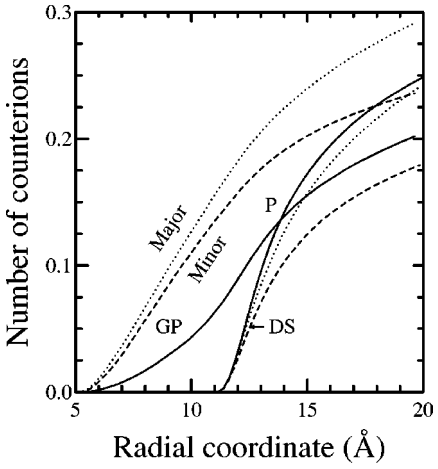


FIG. 12. Variation of the number of counterions in different angular classes (see the text for the class definitions) with the distance to the polyelectrolyte axis for the GP and DS models at 0.05 M salt concentration. The number of ions refer to a DNA base. Phosphates (solid lines), major groove (dotted lines), and minor groove (dashed lines). The curves whose origins are at 5 and 11 Å correspond to the GP and DS models, respectively.

As for coions at high salt concentrations, the GP predicts the population to be in the order major groove≫minor >phosphates. The DS model also predicts a higher popula-

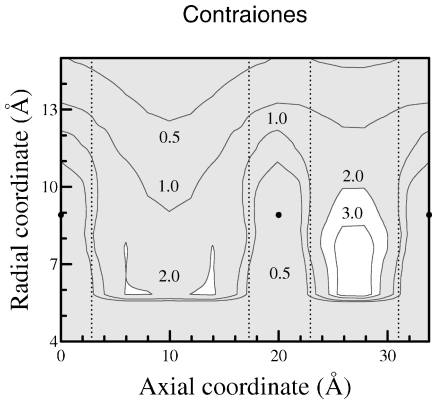


FIG. 13. Net charge profile (at 0.05 M salt concentration) calculated with the FDPB theory.

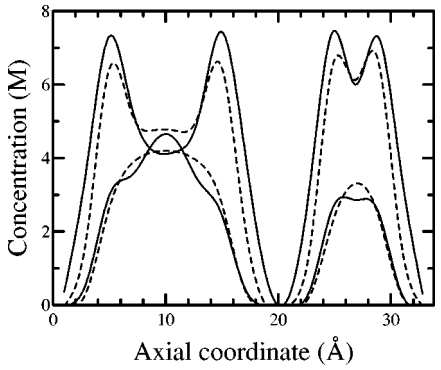


FIG. 15. Concentration profiles of coions and counterions for the GP model at a radial coordinate of 8.9 Å and 4.5 M salt concentration: Monte Carlo simulation (solid lines) and FDPB theory (dashed lines).

tion in the major groove but the the number of coions in the minor groove is now slightly smaller than in the phosphates region. The explanation of this effect is the efficient screening of the phosphates charge by the compact counterion cloud in their proximity in the DS model. In all cases, coions near DNA prefer the major groove region, in which the electrostatic potential is less negative. This is amplified by the arrangement of counterions in the edge of the major groove in the GP model.

Figures 13 and 14 are equivalent to 7 (0.05 M) and 10 (4.5 M), respectively, but present results obtained using the Poisson–Boltzmann theory instead of Monte Carlo simulations. At 0.05 M both techniques give almost indistinguishable results (the small discrepancies at radial coordinates of about 6 Å arise from the fact that we are comparing the results for a hard model with those for a soft one). At high salt the departures increase but they only become qualitatively significant at salt concentrations above 1 M. At 4 M salt concentration, the failure of the FDPB results is severe. The pronounced structure of the charge distribution around DNA shown by the simulations is greatly smoothed out by the Poisson–Boltzmann theory (cf. Figs 10 and 14). Not only are smaller the regions with highly positive net charge in the PB distribution—see, for example, the white areas with net charge concentration above 2.0 M—but the black areas corresponding to negative net charge are completely missing in the latter plot. If one compares the coion and counterion axial distributions separately, as we do in Fig. 15 where the concentration profiles at a radial coordinate of 8.9 Å are shown, the differences are brought out even more. Globally the theory puts too few counterions (with respect to the simulation) around DNA, but in the middle of the major groove—where the Monte Carlo profiles exhibit local charge inversion—the opposite is true so the charge inversion is not predicted by the PB equation. This confirms that alternating charge ion correlations, factor neglected by the PB theory, coupled with steric considerations are major driving forces that shape the ion distribution within the DNA grooves.

Finally, Fig. 16 shows the MC and PB results for the cylindrically averaged ionic distributions at the the higher salt concentration. The counterion curve obtained from simulation data exhibits a double maximum as a consequence of the penetration of ions into the major groove. The double maximum is also predicted by the PB equation but the theory clearly underestimates the counterion profile within the grooves and overestimates it outside the polyion. The MC and PB coion profiles are quite similar at all distances with the significant exception of the region close to the DNA axis where the simulation results show a maximum which is absent in the theoretical calculations.

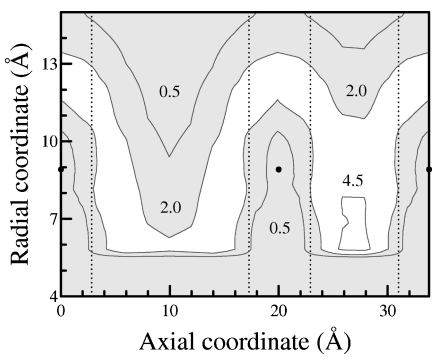


FIG. 14. Net charge profile (at 4.5 M salt concentration) calculated with the FDPB theory.

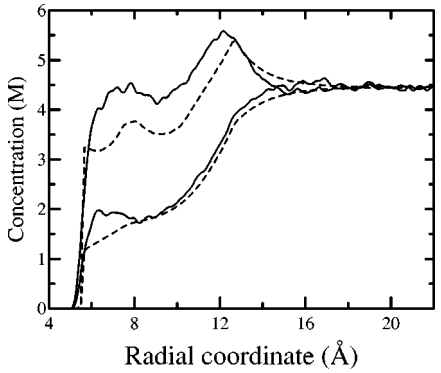


FIG. 16. Cylindrically averaged profiles of coions and counterions for the GP model at 4.5 M salt concentration: Monte Carlo simulation (solid lines) and FDPB theory (dashed lines).

## IV. CONCLUSIONS

In this work we have investigated the detailed three-dimensional structure of the ions around two simple discretely charged *B*-DNA models at the continuum solvent level and with added salt. To simplify the presentation of the results, a helical projection has been introduced which enables the use of only two independent coordinates. It is seen that the small approximation involved in this representation has no effect on the final results. The ionic distribution around the grooved (GP) model has a complex structure far from cylindrical symmetry in the inhomogeneous region extending up to about 20 Å from the DNA axis. The counterions deeply penetrate into the DNA grooves even at very low added salt concentrations. In the minor groove the counterions are preferentially located in the center, whereas they lie at the sides of the major groove, close to the phosphate positions. The coions also enter within the major groove, especially in the systems at high added salt concentrations for which regions of absolute negative charge are predicted within this groove. This can be explained in terms of an arrangement of ions with alternating charges. The coions also penetrate within the minor groove but to a lesser extent, because the alternating arrangement is not possible due to steric hindrance. Thus, counterions always prevail and no charge inversion is found in this region. As the structure observed in our simulations of the GP model strongly depends on the correlations between ions and the electrostatic field created by the polyelectrolyte, its shape and its interactions with other ions, some of the features of the ionic distribution (the local charge inversion) can not be predicted by theories based on approximations which neglect the correlations between the mobile ions such as the Poisson–Boltzmann equation. Nevertheless, aside from this failure, the PB equation gives an acceptable prediction for the ionic profiles even at salt concentrations as high as 1 M.

The DS model leads to completely different and quite unnatural results, as the cylinder core prevents the ions from penetrating DNA. These results and other calculations (in particular, the poor predictions for the *B* to *Z*-DNA transition[73]) cast some doubt on the usefulness of the model since the simple homogeneously charged cylindrical model is able to account satisfactorily for the cylindrically averaged properties.[40] It seems then that for a correct description of the inhomogeneous distribution of ions around DNA (and properties depending on the ionic structure) the models must incorporate two elements, namely, the discrete nature of the DNA charge and its grooved shape. The qualitative prediction of the *B* to *Z*-DNA transition with an ''empty'' DNA model (made of charged spheres at the phosphate positions)[9] seems to indicate that the latter condition can be somewhat relaxed, in the sense that the more important point is to allow the ions to penetrate DNA.

The GP model is thus a simple system fulfilling both requirements. Its predictions are in line with the scarce data available for the ionic distributions in all-atom DNA models.[39] In fact, one of the merits of GP the model is that it makes feasible such calculations in systems with added salt. But the limitations of the model are obvious and they might modify the conclusions reached in this paper. Notably, the model ignores the explicit interactions with the solvent. The DNA hydration may give rise to specific effects such as the spine of hydration in the minor groove, which in turn may affect the ion distributions.[74] Anyway, the GP model results are a good starting point to distinguish effects due to general electrostatic interactions from those that arise from the interactions with water (or other more specific effects).

## ACKNOWLEDGMENTS

This work was partially supported by Grants PB93-0085 and PB96-0588 provided by the Dirección General de Investigación Científica y Tecnológica (DGCICYT) of Spain.

[1] T. E. Creighton, *Proteins: Structure and Molecular Properties* (Freeman, New York, 1993).
[2] M. H. Werner, A. M. Gronenborn, and G. M. Clore, Science **271**, 778 (1996).
[3] W. F. Dove and N. Davidson, J. Mol. Biol. **5**, 467 (1962).
[4] M. T. Record, Jr., S. J. Mazur, P. Melancon, J. H. Roe, S. L. Shaner, and L. Unger, Annu. Rev. Biochem. **50**, 997 (1981).
[5] F. M. Pohl and T. M. Jovin, J. Mol. Biol. **67**, 375 (1972).
[6] T. M. Jovin, D. M. Soumpasis, and L. P. McIntosh, Annu. Rev. Phys. Chem. **38**, 521 (1987).
[7] D. M. Soumpasis and T. M. Jovin, *Nucleic Acids and Molecular Biology, Vol. 1* (Springer-Verlag, Berlin, 1987).
[8] M. A. Frank-Kamenetskii, V. V. Anshelevich, and A. V. Lukashin, Sov. Phys. Usp. **30**, 317 (1987).
[9] J. C. Gil Montoro and J. L. F. Abascal, J. Chem. Phys. **106**, 8239 (1997).
[10] A. R. Rahmouni and R. D. Wells, Science **248**, 359 (1989).
[11] D. G. Pestov, A. Dayn, E. Y. Siyanova, D. L. George, and S. M. Mirkin, Nucleic Acids Res. **19**, 6527 (1991).
[12] R. R. Sinden, *DNA structure and function* (Academic, London, 1994).
[13] A. Katchalsky, Pure Appl. Chem. **26**, 327 (1971).
[14] G. S. Manning, J. Chem. Phys. **51**, 924 (1969).
[15] G. S. Manning, J. Chem. Phys. **51**, 934 (1969).
[16] G. S. Manning, J. Chem. Phys. **51**, 3249 (1969).
[17] G. S. Manning, J. Phys. Chem. **7**, 95 (1977).
[18] T. L. Hill, Arch. Biochem. Biophys. **57**, 229 (1955).
[19] R. A. Marcus, J. Chem. Phys. **23**, 1057 (1955).
[20] P. Mills, C. F. Anderson, and M. T. Record, Jr., J. Phys. Chem. **89**, 3984 (1985).
[21] C. S. Murthy, R. Bacquet, and P. J. Rossky, J. Phys. Chem. **89**, 701 (1985).
[22] P. Mills, M. D. Paulsen, C. F. Anderson, and M. T. Record, Jr., Chem. Phys. Lett. **129**, 155 (1986).
[23] V. Vlachy and A. D. J. Haymet, J. Chem. Phys. **84**, 5874 (1986).
[24] M. D. Paulsen, B. Richey, C. F. Anderson, and M. T. Record, Jr., Chem. Phys. Lett. **139**, 448 (1987).
[25] B. Jayaram, F. M. DiCapua, and D. L. Beveridge, J. Am. Chem. Soc. **113**, 5211 (1991).
[26] J. R. C. van der Maarel, L. C. A. Groot, M. Manderl, W. Jesse, G. Jannink, and V. J. Rodriguez, J. Phys. II **2**, 109 (1992).
[27] L. C. A. Groot, M. E. Kuil, J. C. Leyte, J. R. C. van der Maarel, J. P. Cotton, and G. Jannink, J. Phys. Chem. **98**, 10167 (1994).
[28] Y. Morishima, H. Ohgi, and M. Kamachi, Macromolecules **26**, 4293 (1993).
[29] T. G. Wensel, C. F. Meares, V. Vlachy, and J. B. Matthew, Proc. Natl. Acad. Sci. USA **83**, 3267 (1986).
[30] T. E. Strzelecka and L. R. Randolph, J. Phys. Chem. **96**, 7796 (1992).
[31] P. A. Mills, A. Rashid, and T. L. James, Biopolymers **32**, 1491 (1992).
[32] T. R. Forester and I. R. McDonald, Mol. Phys. **72**, 643 (1991).
[33] R. A. Friedman and M. Mezei, J. Chem. Phys. **102**, 419 (1995).
[34] D. L. Beveridge and G. Ravishanker, Curr. Opin. Struct. Biol. **4**, 246 (1994).
[35] B. Jayaram, N. Aneja, E. Rajasekaran, V. Arora, A. Das, V. Ranganathan, and V. Gupta, J. Sci. Ind. Res. **53**, 88 (1994).
[36] H. L. Gordon and S. Goldman, J. Phys. Chem. **96**, 1921 (1992).
[37] F. Gago and W. G. Richards, Molec. Pharmacol. **37**, 341 (1990).
[38] B. Jayaram, S. Swaminathan, D. L. Beveridge, K. Sharp, and B. Honig, Macromolecules **23**, 3156 (1990).

[39] L. E. Guldbrand, T. R. Forester, and R. M. Lynden-Bell, Mol. Phys. **67**, 473 (1989).
[40] J. C. Gil Montoro and J. L. F. Abascal, J. Chem. Phys. **103**, 8273 (1995).
[41] B. J. Klein and G. R. Pack, Biopolymers **22**, 2331 (1983).
[42] B. Jayaram, K. A. Sharp, and B. Honig, Biopolymers **28**, 975 (1989).
[43] G. Lamm, L. Wong, and G. R. Pack, Biopolymers **34**, 227 (1994).
[44] J. L. Hecht, B. Honig, Y. Shin, and W. L. Hubbell, J. Chem. Phys. **99**, 7782 (1995).
[45] V. K. Misra and B. Honig, Biochemistry **35**, 1115 (1996).
[46] W. Saenger, *Principles of Nucleic Acid Structure* (Springer-Verlag, New York, 1984).
[47] S. Arnott and D. W. Hukins, Biochem. Biophys. Res. Commun. **47**, 1504 (1972).
[48] P. J. Rossky, J. B. Dudowick, B. L. Tembe, and H. L. Friedman, J. Chem. Phys. **73**, 3372 (1980).
[49] P. N. Vorontsov-Velyaminov and A. P. Lyubartsev, Mol. Simul. **9**, 285 (1992).
[50] F. Bresme and J. L. F. Abascal, J. Chem. Phys. **99**, 9037 (1993).
[51] J. L. F. Abascal, F. Bresme, and P. Turq, Mol. Phys. **81**, 143 (1994).
[52] J. C. Gil Montoro, F. Bresme, and J. L. F. Abascal, J. Chem. Phys. **101**, 10892 (1994).
[53] D. M. York, T. Darden, D. Deerfield II, and L. G. Pedersen, Int. J. Quantum Chem. **19**, 145 (1992).
[54] W. F. van Gunsteren, H. J. Berendsen, R. G. Guersten, and H. R. Zwinderman, Ann. (N.Y.) Acad. Sci. **482**, 287 (1986).
[55] J. Conrad, M. Troll, and B. H. Zimm, Biopolymers **27**, 1711 (1988).
[56] C. Tanford and J. G. Kirkwood, J. Am. Chem. Soc. **79**, 5348 (1957).
[57] G. M. Torrie and J. P. Valleau, J. Chem. Phys. **73**, 5807 (1980).
[58] J. C. Gil Montoro and J. L. F. Abascal, Mol. Simul. **14**, 313 (1995).
[59] J. C. Gil Montoro and J. L. F. Abascal, Mol. Phys. **89**, 1071 (1996).
[60] J. D. Jackson, *Classical Electrodynamics* (Wiley, New York, 1967).
[61] R. M. Fuoss, A. Katchalsky, and S. Lifson, Proc. Natl. Acad. Sci. USA **37**, 579 (1951).
[62] A. Brunger, C. L. Brooks, and M. Karplus, Chem. Phys. Lett. **105**, 495 (1984).
[63] C. L. Brooks, B. M. Pettitt, and M. Karplus, J. Chem. Phys. **83**, 5897 (1985).
[64] H. L. Gordon and S. Goldman, Mol. Simul. **3**, 213 (1989).
[65] A. Nicholls and B. Honig, J. Comput. Chem. **12**, 435 (1991).
[66] M. Gilson, K. A. Sharp, and B. Honig, J. Comput. Chem. **9**, 327 (1988).
[67] T. R. Forester, Ph.D. thesis, University of Cambridge, 1988.
[68] M. Troll, D. Roitman, J. Conrad, and B. H. Zimm, Macromolecules **19**, 1186 (1986).
[69] J. B. Matthew and F. M. Richards, Biopolymers **23**, 2743 (1984).
[70] G. R. Pack and B. J. Klein, Biopolymers **23**, 2801 (1984).
[71] J. A. Schellman and D. Stigter, Biopolymers **16**, 1415 (1977).
[72] V. N. Bartenev, E. I. Golovamov, K. A. Kapitonova, M. A. Mokulskii, L. I. Volkova, and I. Y. Skuratovskii, J. Mol. Biol. **169**, 217 (1983).
[73] J. C. Gil Montoro, Ph.D. thesis, Univ. Complutense de Madrid, 1997.
[74] M. A. Young, B. Jayaram, and D. L. Beveridge, J. Am. Chem. Soc. **119**, 59 (1997).